CHAOTIC SIGNALS DENOISING BASED ON ADAPTIVE THRESHOLD MULTI-SYNCHROSQUEEZING TRANSFORM

Chunlu WAN[1,*], Wenqi CHEN[1]

To address the limitation of single-threshold MSST denoising, we propose an improved amplitude thresholding method that incorporates a layered threshold in the MSST framework. First, based on the distribution model of signal and noise coefficients after MSST decomposition, the mean squared error (MSE) formula for the amplitude threshold weighting coefficient in MSST chaotic denoising is derived. Then based on the minimum MSE criterion, the optimal value of the amplitude threshold weighting coefficient is determined. Finally, the layered threshold for MSST chaotic denoising is established based on the optimal threshold weighting coefficient and the noise standard deviation. This method is evaluated using the simulated chaotic signals and monthly sunspot data. The experimental results show that this method can effectively reduce noise in chaotic signals when significantly preserving their intrinsic characteristics. For the Duffing chaotic system, compared with the wavelet threshold method, the SNR can increase by 6.7738 and the RMSE can decrease by 0.2317. Compared with the complete ensemble empirical mode decomposition with adaptive noise method (CEEMDAN), the SNR can increase by 4.6088 and the RMSE can decrease by 0.1993. For the measured sunspot sequence, compared with the wavelet threshold method, the recurrence rate (RR), recurrence rate determinism (RRD), maximum diagonal line length (Lmax) and recurrence trend (RT) after noise reduction by the method proposed can increase by 12.09%, 1.57%, 14.36% and 6.73%, respectively. Compared with the CEEMDAN method, the RR, RRD, Lmax and RT of this method can increase by 7.47%, 0.97%, 6.45% and 4.49%, respectively.

Keywords: multi-synchro squeezing transform, signal denoising, chaotic system, sunspot data analysis

1. Introduction

Since the 1960s, the significant acceleration of progress in nonlinear science have promoted extensive researches on chaotic systems [1]. As a fundamental component of nonlinear science, chaotic theory has been widely explored in various scientific and engineering disciplines, leading to its application in electronics, meteorology, hydrology, and secure communications [2, 3]. However, due to limitations of measurement instruments and environmental interference, measured chaotic signals are often contaminated by different levels of noise [4]. This noise

* Corresponding author, e-mail: 19404425@qq.com
[1] College of Artificial Intelligence, Wuchang University of Technology, Wuhan, 430000, China

disrupts the intrinsic characteristics of chaotic attractors, making it significantly challenging to calculate invariant system parameters such as the Lyapunov exponent, correlation dimension, and Kolmogorov entropy [5]. Noise suppression in chaotic signals is a prerequisite for subsequent processing and applications [6]. Chaotic signals have a wide power spectrum, and their spectral characteristics are similar to noise, which renders traditional noise reduction methods such as Wiener filtering and spectral analysis ineffective. Therefore, developing effective noise reduction methods tailored for chaotic signals is of great significance [6].

The synchro squeezing transform (SST) has been widely applied in the denoising of nonlinear signals [7-12]. Cheng et al. [7] applied SST to surface wave removal in seismic signals and compared it with continuous wavelet transform (CWT), *f-k* filtering methods. Zhou [8] and Chen et al. [9] utilized SST for micro seismic signal denoising and event onset detection, with experimental results demonstrating that SST is better than traditional denoising methods. Yuan et al. [10] applied SST to denoising multivariate signals acquired from multi-channel sensors, proving the effectiveness of the algorithm through experiments. Matthew et al. [11] used SST in low-strain pile foundation testing, achieving separation of pile bottom reflection signals from noise. Bantis et al. [12] used SST to analyze the frequency and damping ratio of noisy signals, achieving favorable results. The performance of SST is better than WT and EMD.

The multi-synchro squeezing transform (MSST) is a new time-frequency analysis method based on SST [13]. MSST improves time-frequency precision by synchro squeezing along the STFT frequency axis, minimizing cross-term interference and effectively mitigating spectral aliasing in the time-frequency analysis of nonlinear and complex signals [14, 15]. MSST also shows strong robustness to noise. Even when a signal is severely contaminated, MSST can still extract clear time-frequency curves and generate largely invariant decomposition results [16]. However, existing MSST denoising algorithms use a single threshold, meaning the same threshold is applied in all decomposition layers of the MSST. After MSST decomposition, the noise intensity varies in different layers of MSST coefficients, making a single-threshold approach unsuitable for effective denoising. To address this limitation, this study extends the existing MSST denoising algorithm for chaotic signals noise suppression. The denoising threshold for each MSST coefficient layer is calculated based on the noise distribution in noisy chaotic signals decomposed by MSST. Accordingly, a layer threshold chaotic signal denoising method based on MSST is proposed.

2. Multi-synchro squeezing transform

2.1. Synchro squeezing transform

Let $x(t)$ be a single-component signal, i.e., $x(t) = A(t)e^{j\varphi(t)}$. The STFT representation of signal $x(t)$ is given as follows [13]:

$$G(t,\omega)=\int_{-\infty}^{\infty}x(u)g(u-t)e^{-i\omega(u-t)}du \tag{1}$$

where $g(u)$ is a window function. If $G(t,\omega)\neq 0$, then the instantaneous frequency (IF) $\omega(t,\omega)$ of the STFT can be approximately expressed as follows:

$$\omega(t,\omega)=\frac{\partial_t G(t,\omega)}{iG(t,\omega)} \tag{2}$$

Fourier synchro squeezing transform (FSST) is expressed as follows [14]:

$$T_s(t,\eta)=\int_{-\infty}^{\infty}G(t,\omega)\delta(\eta-\hat{\omega}(t,\omega))d\omega \tag{3}$$

where δ represents the Dirac function.

2.2. Multi-synchro squeezing transform

The basic idea of MSST is to progressively concentrate the energy of time-frequency analysis by repeatedly applying multiple FSST operations. Assuming the number of iterations is $N(N\geq 2)$, MSST can be expressed as follows [17]:

$$\begin{cases} T_s^{[2]}(t,\eta)=\int_{-\infty}^{\infty}T_s(t,\omega)\delta(\eta-\hat{\omega}(t,\omega))d\omega \\ T_s^{[3]}(t,\eta)=\int_{-\infty}^{\infty}T_s^{[2]}(t,\omega)\delta(\eta-\hat{\omega}(t,\omega))d\omega \\ \cdots \\ T_s^{[N]}(t,\eta)=\int_{-\infty}^{\infty}T_s^{[N-1]}(t,\omega)\delta(\eta-\hat{\omega}(t,\omega))d\omega \end{cases} \tag{4}$$

The k-th component can be reconstructed as follows:

$$f_k(t)=\int_{\{\omega:|\omega-\varphi_k(t)|<d\}}T_s^{[N]}(t,\eta)d\eta,\ 1\leq k\leq K \tag{5}$$

where $\varphi_k(t)$ is the estimated value of $\phi_k'(t)$; d is the compensation factor between $\varphi_k(t)$ and $\phi_k'(t)$, and K represents the pre-defined number of ridges.

3. MSST-based layered threshold for chaotic signals denoising

3.1. MSST threshold denoising

Let the noisy chaotic signal be represented as $\boldsymbol{y}(t)=\boldsymbol{f}(t)+\boldsymbol{n}(t)$, where $\boldsymbol{f}(t)$ denotes the chaotic signal and $\boldsymbol{n}(t)$ represents the noise. In the MSST decomposition, let $\boldsymbol{a}=\{a(i),i=1,2,\mathrm{L}\ ,I\}$ be the scale used in the CWT. Then, the i-th layer coefficient of the noisy chaotic signal after the MSST transform is given as follows:

$$\boldsymbol{W}_y^{a(i)}(t)=\boldsymbol{W}_f^{a(i)}(t)+\boldsymbol{W}_n^{a(i)}(t) \tag{6}$$

It can be seen that MSST determines the coefficients to be retained after denoising based on the magnitude information of the signal coefficients and their relative position to the main frequency curve, expressed as follows:

$$\tilde{\boldsymbol{W}}_y^{a(i)}(t)=\begin{cases}\boldsymbol{W}_y^{a(i)}(t), & |\boldsymbol{W}_y^{a(i)}(t)|>\gamma^{a(i)}\bigcap|\omega^{a(i)}(t)-\phi_k'(t)|<\varepsilon\\ 0, & else\end{cases} \tag{7}$$

where $\gamma^{a(i)}$ is the magnitude threshold used in MSST denoising, and ε is the frequency threshold for denoising.

3.2. Calculation of MSST layered denoising threshold

From Eq. (6), let the coefficients after threshold-based denoising be:

$$\boldsymbol{W}_{y,d}^{a(i)}(t)=\boldsymbol{W}_{f,d}^{a(i)}(t)+\boldsymbol{W}_{n,d}^{a(i)}(t) \tag{8}$$

Chaotic signal denoising aims to ensure that the denoised signal is as close as possible to the true signal, that is, $\boldsymbol{W}_{y,d}^{a(i)}(t)$ should approximate $\boldsymbol{W}_{f,d}^{a(i)}(t)$ as closely as possible. The objective is to determine an appropriate $c^{a(i)}$ so that the layered threshold $\gamma^{a(i)}=c^{a(i)}\sigma_n$ minimizes the MSE between the denoised coefficients $W_{y,d}^{a(i)}(t)$ and $W_{f,d}^{a(i)}(t)$ and the true chaotic signal coefficients, i.e., $E[\boldsymbol{W}_{y,d}^{a(i)}-\boldsymbol{W}_{f,d}^{a(i)}]^2$ is minimized.

$$\begin{aligned}&E[\boldsymbol{W}_{y,d}^{a(i)}-W_f^{a(i)}]^2=E[\boldsymbol{W}_{y,d}^{a(i)}]^2+E[\boldsymbol{W}_f^{a(i)}]^2-2E[\boldsymbol{W}_{y,d}^{a(i)}\cdot\boldsymbol{W}_f^{a(i)}]\\&=E[\boldsymbol{W}_{y,d}^{a(i)}]^2+E[\boldsymbol{W}_f^{a(i)}]^2-2E[\boldsymbol{W}_{y,d}^{a(i)}\cdot\boldsymbol{W}_y^{a(i)}]+2E[(\boldsymbol{W}_{f,d}^{a(i)}+\boldsymbol{W}_{n,d}^{a(i)})\cdot\boldsymbol{W}_n^{a(i)}]\end{aligned} \tag{9}$$

Since the noise and signal are mutually independent, $E[\boldsymbol{W}_{f,d}^{a(i)}\cdot\boldsymbol{W}_n^{a(i)}]=0$. The above equation can be simplified as follows:

$$E[\boldsymbol{W}_{y,d}^{a(i)}-W_f^{a(i)}]^2=E[\boldsymbol{W}_{y,d}^{a(i)}]^2+E[\boldsymbol{W}_f^{a(i)}]^2-2E[\boldsymbol{W}_{y,d}^{a(i)}\cdot\boldsymbol{W}_y^{a(i)}]+2E[\boldsymbol{W}_{n,d}^{a(i)}\cdot\boldsymbol{W}_n^{a(i)}] \tag{10}$$

From the denoising Eq. (7), it can be seen that:

$$\begin{cases}\boldsymbol{W}_{f,d}^{a(i)}(t)=\boldsymbol{W}_f^{a(i)}(t),\ \boldsymbol{W}_{n,d}^{a(i)}(t)=\boldsymbol{W}_n^{a(i)}(t), & |\boldsymbol{W}_y^{a(i)}(t)|>c^{a(i)}\sigma_n\bigcap|\omega^{a(i)}(t)-\phi_k'(t)|<\varepsilon\\ \boldsymbol{W}_{f,d}^{a(i)}(t)=0,\ \boldsymbol{W}_{n,d}^{a(i)}(t)=0, & |\boldsymbol{W}_y^{a(i)}(t)|\le c^{a(i)}\sigma_n\ or\ |\omega^{a(i)}(t)-\phi_k'(t)|\ge\varepsilon\end{cases} \tag{11}$$

Substituting $E[\boldsymbol{W}_{y,d}^{a(i)}\cdot\boldsymbol{W}_y^{a(i)}]=E[\boldsymbol{W}_{y,d}^{a(i)}\cdot\boldsymbol{W}_{y,d}^{a(i)}]$ and $E[\boldsymbol{W}_{n,d}^{a(i)}\cdot\boldsymbol{W}_n^{a(i)}]=E[\boldsymbol{W}_{n,d}^{a(i)}\cdot\boldsymbol{W}_{n,d}^{a(i)}]$ into Eq. (10), then:

$$E[\boldsymbol{W}_{y,d}^{a(i)}-W_f^{a(i)}]^2=E[\boldsymbol{W}_f^{a(i)}]^2-E[\boldsymbol{W}_{y,d}^{a(i)}]^2+2E[\boldsymbol{W}_{n,d}^{a(i)}]^2 \tag{12}$$

The error function $e(c^{a(i)},\varepsilon)=E[\boldsymbol{W}_{y,d}^{a(i)}-\boldsymbol{W}_f^{a(i)}]^2$ can be written as:

$$e(c^{a(i)},\varepsilon)=2E[\boldsymbol{W}_{n,d}^{a(i)}]^2-E[\boldsymbol{W}_{y,d}^{a(i)}]^2 \tag{13}$$

In SST chaotic denoising, the frequency threshold ε is set as a constant **Error! Reference source not found.**, $e(c^{a(i)},\varepsilon)=e(c^{a(i)})$, and the error function can be expressed as:

$$e(c^{a(i)})=2E[\boldsymbol{W}_{n,d}^{a(i)}]^2-E[\boldsymbol{W}_{y,d}^{a(i)}]^2 \tag{14}$$

From Eq. (13), finding the optimal magnitude threshold $\gamma^{a(i)}=c^{a(i)}\sigma_n$ is equivalent to determining the value of $c^{a(i)}$ that minimizes $e(c^{a(i)})$, that is,

$$\min_{c^{a(i)}} e(c^{a(i)})=2E[\boldsymbol{W}_{n,d}^{a(i)}]^2-E[\boldsymbol{W}_{y,d}^{a(i)}]^2 \tag{15}$$

where $E[\boldsymbol{W}_{y,d}^{a(i)}]^2$ can be directly obtained from the MSST coefficients. To find $\min_{c^{a(i)}} e(c^{a(i)})$, it is sufficient to calculate $E[\boldsymbol{W}_{n,d}^{a(i)}]^2$. If $\boldsymbol{W}_{n,d}^{a(i)}(t)$ and $\boldsymbol{W}_{n}^{a(i)}(t)$ are rearranged in ascending order of absolute value, then the first k points of $\boldsymbol{W}_{n,d}^{a(i)}(t)$ are zero, and the remaining $N-k$ points are identical to those in $\boldsymbol{W}_{n}^{a(i)}(t)$,

$$E[\boldsymbol{W}_{n,d}^{a(i)}]^2=\frac{1}{N}\sum_{t=1}^{N}[\boldsymbol{W}_{n,d}^{a(i)}(t)]^2=\frac{1}{N}\sum_{t=1}^{N}[\boldsymbol{W}_{n}^{a(i)}(t)]^2-\frac{1}{N}\sum_{t=1}^{k}[\boldsymbol{W}_{n}^{a(i)}(t)]^2 \tag{16}$$

Since $\frac{1}{N}\sum_{t=1}^{N}[\boldsymbol{W}_{n}^{a(i)}(t)]^2=\sigma_n^2$,

$$E[\boldsymbol{W}_{n,d}^{a(i)}]^2=\sigma_n^2-\frac{1}{N}\sum_{t=1}^{k}[\boldsymbol{W}_{n}^{a(i)}(t)]^2 \tag{17}$$

According to Ref. **Error! Reference source not found.**, when the noisy signal coefficients satisfy $|\boldsymbol{W}_{y}^{a(i)}(t)|<\gamma^{a(i)}$, the noise coefficients $|\boldsymbol{W}_{n}^{a(i)}(t)|<\gamma^{a(i)}$ hold almost true everywhere:

$$\frac{1}{N}\sum_{t=1}^{k}[\boldsymbol{W}_{n}^{a(i)}(t)]^2\approx E\left[(\boldsymbol{W}_{n}^{a(i)})^2\,\middle|\,|\boldsymbol{W}_{y}^{a(i)}|<\gamma^{a(i)}\right] \tag{18}$$

To better prove that the MSST coefficients of pure chaotic signals follow a Gaussian distribution and those of noisy signals follow a Laplacian distribution, the skewness and kurtosis of the MSST coefficients of each layer are calculated respectively. The results are shown in Table 1.

Table 1

Skewness and kurtosis of MSST coefficient

Layer number	Noiseless chaotic signal		Noisy chaotic signal	
	skewness	kurtosis	skewness	kurtosis
J=1	0.0096	0.0167	0.0117	3.1435
J=2	0.0117	0.0084	0.0168	2.9899
J=3	0.0128	0.0074	0.0144	3.0042
J=4	0.0086	0.0125	0.0071	3.1508

For the MSST coefficients of chaotic signals containing noise, the skewness is all close to 0 (with an average value of 0.0125), and the kurtosis is approximately equal to 3(with an average value of 3.0721). The Laplace distribution is suitable for modeling the distribution of MSST coefficients in noisy signals. Therefore, the mixed coefficients $\boldsymbol{W}_y^{a(i)}$ can be assumed to approximately follow a Laplace distribution, i.e., $\boldsymbol{W}_n^{a(i)}$: $N(0,\sigma_n^2)$, $\boldsymbol{W}_y^{a(i)}$: $Laplace(0,\sigma_y)$. Substituting this into Eq. (18), then:

$$\min_{c^{a(i)}} e(c^{a(i)}) = \min_{c^{a(i)}} 2\left[\sigma_n^2 - \frac{1}{\sqrt{2\pi}\sigma_n L(c^{a(i)})}\int_{-c^{a(i)}\sigma_n}^{c^{a(i)}\sigma_n} w^2 e^{-w^2/(2\sigma_n^2)} dw\right] - E[\boldsymbol{W}_y^{a(i)}]^2 \quad (19)$$

In this study, the range of $c^{a(i)}$ is set to $c^{a(i)} \in [1.5, 6.5]$, with values taken sequentially at a step size of 0.01. The layered threshold $\gamma^{a(i)} = c^{a(i)}\sigma_n$ is calculated, and denoising of the i-th layer MSST coefficients is carried out using Eq. (7). The denoised chaotic signal $\boldsymbol{y}_d(t)$ is reconstructed by applying Eq. (5) to the denoised coefficients of each layer.

4. Simulation experiments and analysis

To evaluate the performance of the MSST-based layered threshold denoising method, experiments were conducted on simulated chaotic signals and measured monthly sunspot signals. The WT method **Error! Reference source not found.**, the CEEMDAN thresholding denoising method **Error! Reference source not found.**, and the proposed method were applied to chaotic signals for denoising analysis. For simulated chaotic signals, the denoising performance was evaluated based on the following two aspects: (1) Phase portraits and waveforms of the denoised signals; (2) Signal-to-noise ratio (SNR) and Root mean squared error (RMSE) of the denoised signals. For the measured monthly sunspot series, denoising was assessed based on the following two aspects due to the lack of noise free raw signals: (1) Two-dimensional phase space comparison of the denoised signal; (2) Recurrence plots. To quantitatively assess the denoising performance using recurrence plots, the quantitative recurrence plot indicators: Recurrence Rate (RR), Determinism (DET), Longest Diagonal Line Length ($L_{\max}$) and Recurrence Trend (RT), are provided [20, 21].

4.1. Denoising of simulated Duffing chaotic signals

The chaotic signal can be generated by the Duffing system:

$$x'' + cx' - f_0^2 x + dx^3 = P\cos(ft) \quad (20)$$

where f_0 is the natural angular frequency of the system; c is the damping coefficient; d is the linear parameter; P and f correspond to the external excitation amplitude and external excitation frequency, respectively. The fourth-order Runge-Kutta method is used for solution, with the parameters set as: $c = 0.05$, $f_0^2 = 0.2$, $d = 1$, $f = 2$, $P = 10$, and the sampling interval as $\Delta t = 0.006$. A total of 20,000 data points were generated, with the last 5,000 data points used as experimental data. Gaussian white noise with SNRs of -5 dB, 0 dB, 5 dB, 10 dB, 15 dB, and 20 dB were added to the experimental data.

Table 2 shows the SNR and RMSE of denoising signals by three methods when the input SNR is 5 dB. It can be observed that the proposed method achieves notable improvements in SNR and RMSE. Compared with the wavelet thresholding method, the proposed method can improve the SNR by about 6.7738 and reduce the RMSE by about 0.2317. Compared with the CEEMDAN denoising method, the SNR can increase by about 4.6088, and the RMSE can decrease by about 0.1993.

Table 2

SNR (dB) and RMSE of denoised chaotic signals under different noise levels

Input SNR	WT method	CEEMDAN method	The proposed method
	SNR/RMSE	SNR/RMSE	SNR/RMSE
-5	7.9846 ± 0.3124/0.8126 ± 0.0244	8.86997 ± 0.2264/0.7552 ± 0.0193	**13.8229 ± 0.2395/0.4913 ± 0.0147**
0	9.6105 ± 0.2985/0.6883 ± 0.0198	11.3827 ± 0.3192/0.5976 ± 0.0162	**16.2362 ± 0.2849/0.3176 ± 0.0085**
5	13.3486 ± 0.3567/0.5335 ± 0.0143	15.1612 ± 0.3862/0.4825 ± 0.0123	**20.1809 ± 0.4099/0.2125 ± 0.0065**
10	17.0550 ± 0.4604/0.4870 ± 0.0131	19.6562 ± 0.4652/0.3638 ± 0.0106	**25.9117 ± 0.5022/0.1838 ± 0.0056**
15	20.9114 ± 0.3971/0.3296 ± 0.0051	23.8719 ± 0.3796/0.3162 ± 0.0048	**27.7002 ± 0.3021/0.1266 ± 0.0033**
20	25.7420 ± 0.4217/0.2146 ± 0.0039	28.7002 ± 0.3944/0.1728 ± 0.0031	**31.4432 ± 0.3332/0.0406 ± 0.0024**

To evaluate the denoising performance of different algorithms from the perspective of chaotic characteristics, Fig. 1 shows the chaotic attractor phase portraits of denoised signals obtained using the three methods when the input SNR is 5dB. Fig. 1(a) shows the phase portrait of the noisy chaotic data, and Figs. 1(b)-

(d) show the phase portraits obtained after denoising using the wavelet thresholding method, the CEEMDAN denoising method, and the proposed method, respectively. As shown in Fig. 1, the chaotic attractor phase portraits of signals denoised by wavelet thresholding and CEEMDAN methods have low similarity to the original Duffing signal attractor, characterized by irregular and non-smooth trajectories. In contrast, the phase portrait of the signal denoised using the proposed method shows smoother and more regular attractor trajectories, demonstrating a higher similarity to the original Duffing signal attractor. Since the chaotic attractor structure is mainly distorted by noise, Fig. 1 indicates that the proposed denoising method preserves the chaotic attractor structure more effectively.

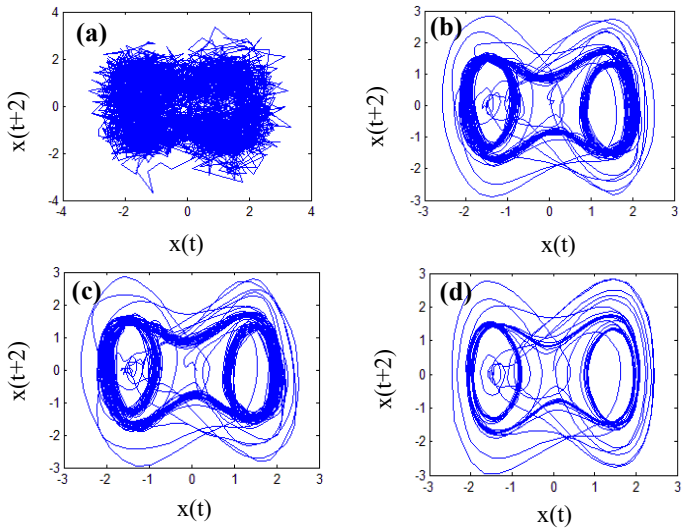

Fig. 1 Phase graphs of noisy and denoisied Dufffing signal: (a) phase graph of noisy Duffing signal; (b) denoised phase graph by wavelet; (c) denoised phase graph by CEEMDAN; (d) denoised phase graph of the proposed method

4.2. Noise reduction of measured sunspot signals

The activity of sunspots has a significant impact on the Earth's magnetic field and climate. Using chaos theory to analyze sunspot activity has become an important research approach. However, noise is inevitably present in measured sunspot series, and eliminating noise is a fundamental step for further processing of sunspot data. In this study, the monthly sunspot series provided by NASA, including the period from January 1749 to December 2015 (http://solarscience.msfc.nasa.gov/green-wch.shtml), was selected as the experimental dataset. The wavelet thresholding method, the CEEMDAN method, and the proposed method were applied to denoise the sunspot data. The chaotic attractor of the sunspot series before and after denoising are shown in Fig. 2.

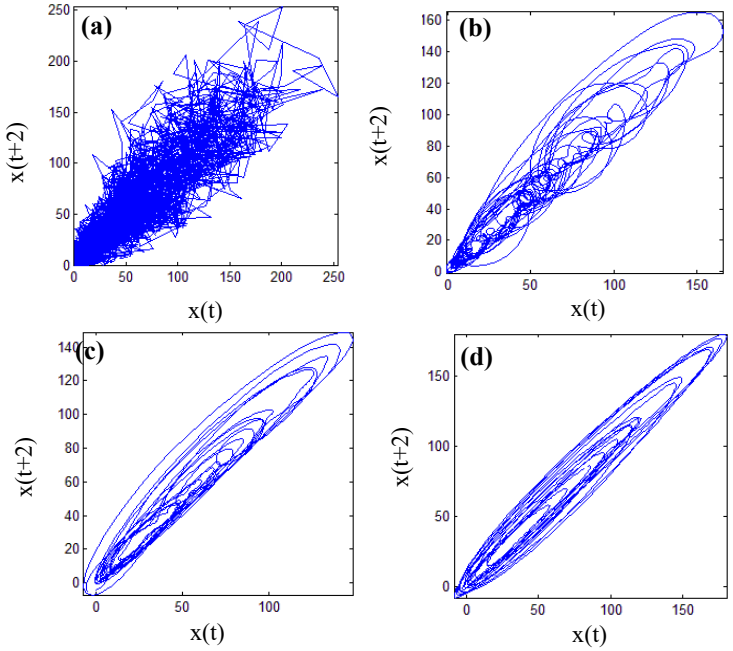

Fig. 2 Denoised phase graphs of monthly sunspot signal: (a) phase graph of original signal; (b) denoised phase graph by wavelet; (c) denoised phase graph by CEEMDAN; (d) denoised phase graph of the proposed method

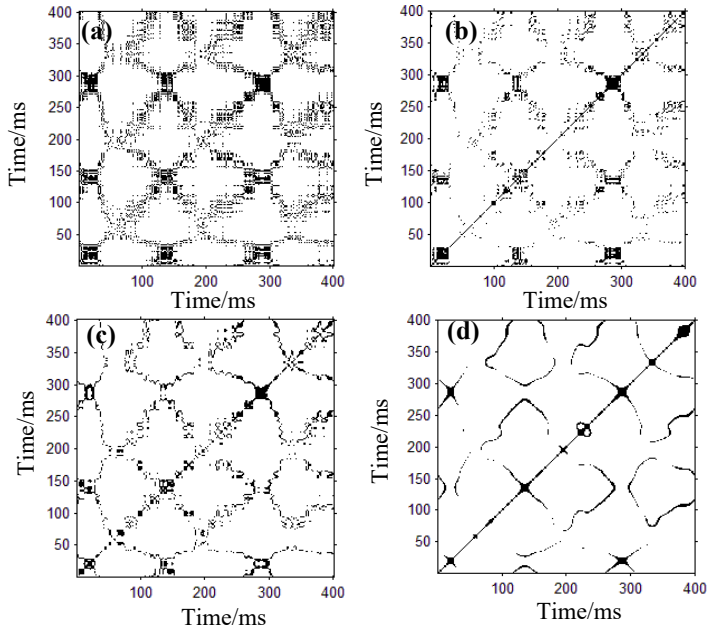

Fig. 3 Denoised recursive graphs of monthly sunspot: (a) recursive graph of original signal; (b) recursive graph by wavelet; (c) recursive graph by CEEMDAN; (d) recursive graph of the proposed method

As shown in Fig. 2(a), due to noise interference, the chaotic attractor phase portrait of the measured monthly sunspot signal appears highly disordered, with unsmooth and irregular attractor trajectories lacking a well-defined geometric structure. As shown in Figs. 2(b) and 2(c), after denoising with the wavelet thresholding method and the CEEMDAN method, the chaotic attractor trajectories of the sunspot signal become clearer and have some regularity. However, the trajectories remain somewhat disordered, and their geometric structure is not entirely well-defined. From Fig. 2(d), it is evident that after denoising with the proposed method, the chaotic attractor trajectories of the sunspot signal become even clearer and more structured, effectively revealing the geometric structure of the chaotic attractor.

To analyze the recurrence plots of the denoised monthly sunspot series, the embedding dimension was set to $m = 5$, the time delay to $\tau = 1$, and critical distance to $r = 5$. Fig. 3 shows the recurrence plots of the sunspot series before and after denoising, including the period from September 1982 to December 2015 (a total of 400 months). Table 3 provides a quantitative analysis of the recurrence plot indicators. From the quantitative indicators in Table 3, it can be seen that after denoising with the proposed method, the recurrence rate (RR), recurrence rate determinism (RRD), maximum diagonal line length ($L_{\max}$), and recurrence trend (RT) all improve significantly compared to the WT method and CEEMDAN method. Compared with the wavelet threshold method, the RR, RRD, $L_{\max}$ and RT after noise reduction by the proposed method have increased by 12.09%, 1.57%, 14.36% and 6.73% respectively. Compared with the CEEMDAN method, the RR, RRD, $L_{\max}$ and RT of the proposed method have increased by 7.47%, 0.97%, 6.45% and 4.49% respectively. Therefore, for the measured monthly sunspot series, this method can achieve effective denoising, showing notable improvements compared to the WT method and CEEMDAN method [22, 23].

Table 3

Quantitative analysis of sunspot recurrence plots

	RR	RRD	Lmax	RT
Measured monthly sunspot Series	0.0067	0.9525	18	0.0012
WT method	0.0488	0.9753	202	0.0327
CEEMDAN method	0.0509	0.9811	217	0.0334
The proposed method	**0.0547**	**0.9906**	**231**	**0.0349**

5. Conclusion

This study introduces an MSST-based layered thresholding method for chaotic signal denoising based on the minimum MSE criterion. It is improved significantly compared to the traditional MSST single-threshold method. The optimal hierarchical threshold is determined by using the minimum MSE criterion

based on the distribution model of the MSST coefficients of noise and chaotic signals. To verify the effectiveness of this method, denoising experiments were conducted on simulated chaotic signals and measured monthly sunspot signals. The experimental results show that this method can filter out the noise in chaotic signals more effectively. Moreover, the phase diagram of the denoised signal can more clearly restore the intrinsic topological structure of the attractor. However, this study only considers amplitude-based layered thresholding in MSST denoising, and the frequency threshold is still applied as a traditional single threshold without computing a layered frequency threshold.

REFERENCES

[1] *G. Feng, F. Hui*, Chaos identification and parameter optimization for vibration suppression in composite bistable structures, Mechanics Research Communications, Vol. **135**, article no. 104236, 2024. Doi: 10.1016/j.mechrescom.2023.104236.

[2] *G. Zhang, C.F. Li, X.Y. Xiong*, Analysis and comparison of four signal processing schemes for noise reduction in chaotic communication systems and application of LDPC code, Chaos, Solitons & Fractals, Vol. **186**, article no. 115184, 2024. Doi: 10.1016/j.chaos.2024.115184.

[3] *Y. Zhou, P.Y. Zhao, Y.J. Guo*, Melnikov analysis of chaotic dynamics in an impact oscillator system, International Journal of Non-Linear Mechanics, Vol. **171**, article no. 105027, 2025. Doi: 10.1016/j.ijnonlinmec.2025.105027.

[4] *C. Wang, H. Lin, M. Yang, X.L. Fu, Y. Yuan, Z.W. Wang*, A novel chaotic time series wind power point and interval prediction method based on data denoising strategy and improved coati optimization algorithm. Chaos, Solitons & Fractals, Vol. **187**, article no. 115442, 2024. Doi: 10.1016/j.chaos.2024.115442.

[5] *Z.F. Liu, R.D. Zhang, Y.J. Wang, H.W. Zhang, G. Wang, Y. Zhang*, Continuous discrete minimum error entropy Kalman filter in non-Gaussian noises system. Digital Signal Processing, Vol. **156**, article no. 104846, 2025. Doi: 10.1016/j.dsp.2024.104846.

[6] *S.T. Lou, J.R. Deng, S.X. Lyu*, Chaotic signal denoising based on simplified convolutional denoising auto-encoder. Chaos, Solitons & Fractals, Vol. **161**, article no. 112333, 2022. Doi: 10.1016/j.chaos.2022.112333.

[7] *X.H. Cheng, A.M. Wang, Z.W. Li, L. Yuan, Y.J. Xiao*, An Enhanced Version of Second-Order Synchrosqueezing Transform Combined with Time-Frequency Image Texture Features to Detect Faults in Bearings, Shock and Vibration, Vol. **2021**, pp. 1-20, 2021. Doi: 10.1155/2021/5589825.

[8] *C. Zhou, H.R. Cao, X.S. Wang, J.M. Ding*, Second-order Iterative Time-rearrangement Synchrosqueezing Transform and its application to rolling bearing fault diagnosis, Measurement, Vol. **190**, article no. 110730, 2022. Doi: 10.1016/j.measurement.2022.110730.

[9] *S.Y. Chen, Y.J. Xue, L. Huang*, Application of second order multi-synchrosqueezing transform for seismic data analysis, Digital Signal Processing, Vol. **148**, article no. 104436, 2024. Doi: 10.1016/j.dsp.2024.104436.

[10] *J. Yuan, Z. Yao, H.M. Jiang, Y.H. Weng, Q. Zhao, W.Y. Hu*, Multi-lifting synchrosqueezing transform for nonstationary signal analysis of rotating machinery, Measurement, Vol. **191**, article no. 110758, 2022. Doi: 10.1016/j.measurement.2022.110758.

[11] *D.E. Matthew, H.R. Cao, J.H. Shi*, Advancing chatter detection: Harnessing the strength of wavelet synchrosqueezing transform and Hilbert-Huang transform techniques, Journal of Manufacturing Processes, Vol. **127**, pp. 613-630, 2024. Doi: 10.1016/j.jmapro.2024.07.092.

[12] *J.C. Bantis, E. Miranda*, Evaluation of random-vibration procedures to estimate response spectral ordinates on soft soil sites from fourier amplitude spectra, Soil Dynamics and Earthquake Engineering, Vol. **166**, article no. 107776, 2023. Doi: 10.1016/j.soildyn.2023.107776.

[13] *C.J. Li, H.Y. Deng, S.Y. Yin, C.M. Wang, Y.F. Zhu*, sEMG signal filtering study using synchrosqueezing wavelet transform with differential evolution optimized threshold, Results in Engineering, Vol. **18**, article no. 101150, 2023. Doi: 10.1016/j.rineng.2023.101150.

[14] *E. Marchi, M. Cervetto, C. Galarza*, Adaptive synchrosqueezing wavelet transform for real-time applications, Digital Signal Processing, Vol. **140**, article no. 104133, 2023. Doi: 10.1016/j.dsp.2023.104133.

[15] *Y. Guo, L. Yang*, An optimization synchrosqueezed fractional wavelet transform for TFF analysis and its applications, Digital Signal Processing, Vol. **156**, article no. 104819, 2025. Doi: 10.1016/j.dsp.2024.104819.

[16] *W.T. Li, Z.T. Zhang, F. Auger, X.X. Zhu*, Theoretical analysis of time-reassigned synchrosqueezing wavelet transform, Applied Mathematics Letters, Vol. **132**, article no. 108141, 2022. Doi: 10.1016/j.aml.2022.108141.

[17] *J.L. Liu, R. Chen, F.Q. Qiu, A.H. Yu, W.T. Zheng, S.P. Wu*, Structural instantaneous frequency identification of non-stationary signals using GDAVMD and MSST, Structures, Vol. **72**, article no. 108234, 2025. Doi: 10.1016/j.istruc.2025.108234.

[18] *J.R. Yang, S.F. Yan, L.L. Mao, Z.P. Sui, W. Wang, D. Zeng*, Underwater acoustic signal denoising based on sparse TQWT and wavelet thresholding, Digital Signal Processing, Vol. **153**, article no. 104601, 2024. Doi: 10.1016/j.dsp.2024.104601.

[19] *G.H. Li, Y.Y. Han, H. Yang*, A new underwater acoustic signal denoising method based on modified uniform phase empirical mode decomposition, hierarchical amplitude-aware permutation entropy, and optimized improved wavelet threshold denoising, Ocean Engineering, Vol. **293**, article no. 116629, 2024. Doi: 10.1016/j.oceaneng.2023.116629.

[20] *Y. Zou, R.V. Donner, N. Marwan, J.F. Donges, J. Kurths*, Complex network approaches to nonlinear time series analysis, Physics Reports, Vol. **787**, article no.1-97, 2019. Doi: 10.1016/j.physrep.2018.10.005.

[21] *Q. He, F.S. Yu*, Trend recurrence analysis and time series classification via trend fuzzy granular recurrence plot method, Chaos, Solitons & Fractals, Vol. **176**, article no. 114158, 2023. Doi: 10.1016/j.chaos.2023.114158.

[22] *X.L. Yang, W.B. Wang*, Chaotic signal denoising based on energy selection TQWT and adaptive SVD, Scientific Reports, Vol. **13,** article no. 1873, 2023. Doi: 10.1038/s41598-023-45811-y.

[23] *G. Yu, Z.H. Wang, P. Zhao*, Multisynchrosqueezing Transform, IEEE Transactions on Industrial Electronics, Vol. **7**, pp. 5441-5455, 2019. Doi: 10.1109/TIE.2018.2868296.